Chemistry–A European Journal

Research Article
doi.org/10.1002/chem.202303380

Chemistry Europe
European Chemical
Societies Publishing

www.chemeurj.org

Quo Vadis CO$_2$ Activation: Catalytic Reduction of CO$_2$ to Methanol Using Aluminum and Gallium/Carbon-based Ambiphiles

Felix Krämer,[a] Jan Paradies,[b] Israel Fernández,*[c] and Frank Breher*[a]

Dedicated to Prof. Lars Wesemann on the occasion of his 60th birthday

We report on so-called "hidden FLPs" (FLP: frustrated Lewis pair) consisting of a phosphorus ylide featuring a group 13 fragment in the *ortho* position of a phenyl ring scaffold to form five-membered ring structures. Although the formation of the Lewis acid/base adducts was observed in the solid state, most of the title compounds readily react with carbon dioxide to provide stable insertion products. Strikingly, 0.3–3.0 mol% of the reported aluminum and gallium/carbon-based ambiphiles catalyze the reduction of CO$_2$ to methanol with satisfactory high selectivity and yields using pinacol borane as stoichiometric reduction equivalent. Comprehensive computational studies provided valuable mechanistic insights and shed more light on activity differences.

Introduction

The use of fossil fuels to meet the world's energy needs and as a means of accessing chemical feedstocks is leading to a steady increase in carbon dioxide (CO$_2$) emissions. CO$_2$ levels in the atmosphere currently stand at 418.17 parts per million, as measured at the Mauna Loa Baseline Observatory on September 14, 2023.[1] CO$_2$ is considered a sustainable alternative C1 feedstock for fossil fuel-derived carbon monoxide (CO) because it is abundant, inexpensive, and non-toxic. A variety of compounds can be produced from CO$_2$, including basic chemicals, polymers, and fuels.[2] However, the promising use of CO$_2$ as a C1 synthon faces significant practical challenges caused by its high thermodynamic stability.

The development of stable, low-cost, active, and selective catalysts that operate under mild conditions is of great interest to industry. On account of the significant interest in abundant main-group element catalysts in green chemistry and environmental protection, aluminum compounds gained a lot of attention in the last two decades.[3] This led to the increased use of aluminum compounds in catalytic reactions, as recently summarized in a review article by Roesky and co-workers.[4]

Two aluminum-based examples of the catalytic reduction of CO$_2$ to methanol were described by Inoue[5a] and So.[5b] The reported aluminum hydride derivatives (Scheme 1) showed catalytic activities with catalyst loadings between 5 and 10 mol% after initial hydroalumination of CO$_2$ and further

[a] Dr. F. Krämer, Prof. Dr. F. Breher
Institute of Inorganic Chemistry
Karlsruhe Institute of Technology (KIT)
Engesserstraße 15, 76131 Karlsruhe (Germany)
E-mail: breher@kit.edu
Homepage: http://www.aoc.kit.edu/breher/

[b] Prof. Dr. J. Paradies
Chemistry Department
Paderborn University
Warburger Str. 100, 33098 Paderborn (Germany)

[c] Prof. Dr. I. Fernández
Departamento de Química Orgánica I, Facultad de Ciencias Químicas and Centro de Innovación en Química Avanzada (ORFEO-CINQA)
Universidad Complutense de Madrid
28040 Madrid (Spain)
E-mail: israel@quim.ucm.es
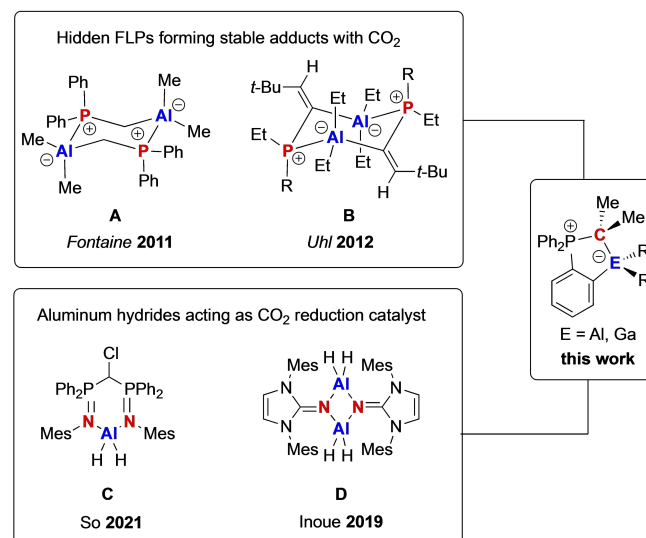
Scheme 1. Two selected examples for hidden Al/P-based FLPs **A** and **B** that form stable adducts with CO$_2$ and Al-hydrides **C** and **D** that act as reduction catalysts for CO$_2$.

Chem. Eur. J. **2023**, e202303380 (1 of 10)

© 2023 The Authors. Chemistry - A European Journal published by Wiley-VCH GmbH

Chemistry–A European Journal

Research Article
doi.org/10.1002/chem.202303380

Chemistry Europe
European Chemical
Societies Publishing

reaction with boranes.[5] Overviews of metal-free reductions of CO_2 were published by Fontaine and Stephan as well as Wirth and Melen.[6] Common FLP-systems consisting of B/P,[7] B/N,[8] Al/P[9] or Si/N[10] Lewis acid/Lewis base combinations reduce CO_2 in the presence of hydroboranes to methanol. Quite recently, Wang and Mo reported the geometrically constrained bis(silylene)-stabilized borylene, which activates C=O, N–H and P–P bonds in a cooperative manner. They further showed the catalytic activity in the reduction of CO_2 to the corresponding N-formamides in the presence of amines and HBpin.[11]

The combination of a carbon-based Lewis base and an aluminum-based Lewis acid is uncommon in the field of FLP chemistry.[12] At variance, a whole series of hidden frustrated Lewis pairs with phosphorus or nitrogen bases are known (two selected examples are given in Scheme 1, top).[13] Interestingly, phosphorus ylides have proven to be valuable carbon Lewis bases for the stabilization of highly reactive compounds and small molecule activation chemistry.[14] Furthermore, we confirmed most recently that the cooperative action of an aluminum Lewis acid and a Lewis basic phosphorus ylide allows the activation of the N–H bond in NH_3.[15] As already shown by Schlosser et al. and Sundermeyer et al., non-stabilized phosphorus ylides $Ph_3PC(R^1)H$ (R^1 = alkyl, aryl) can be metallated in ortho-position on one of the phenyl groups.[16] This reactivity was exploited in this work to prepare ortho-aluminum- and ortho-gallium-substituted phosphorus ylides (referred to as o-AlCPs/o-GaCPs in the following) continuing our most recent work in that field of chemistry.[15] In this article, we report on the reactivity of these species with CO_2 and their successful application as catalysts for the reduction of CO_2 to methanol.

Results and Discussion

As a starting compound for the preparation of o-AlCPs, the ortho-lithiated ylide (2-Li-C_6H_4)Ph_2PCMe_2 (**1**) was generated from the readily available ylide Ph_3PCMe_2 and t-BuLi, as described recently.[15] To prepare the o-AlCPs (2-{AlR$_2$}-C_6H_4)Ph_2PCMe_2 (R=Me (**2^{Me}**), Et (**2^{Et}**), t-Bu (**2^{tBu}**),[15] Mes (**2^{Mes}**) and C_6F_5 (**2^{C6F5}**)), **1** was reacted with the corresponding dialkyl aluminum chlorides or bromides (R$_2$AlX with R=Me, Et, t-Bu, Mes, C_6F_5) in toluene (Scheme 2). Recrystallization from hexane or cyclopentane afforded the title compounds in pure form in yields ranging from 25 to 66%.
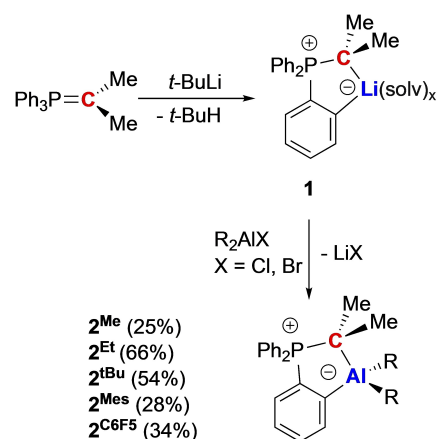
Scheme 2. Reactions of **1** with R$_2$AlX (R=Me, Et, t-Bu,[15] Mes, C_6F_5; X=Cl, Br) to the o-AlCPs **2^R** in toluene at RT.

Crystals of all o-AlCPs **2^R** were investigated by X-ray structure analysis. The molecular structure of **2^{Me}** in the solid state is shown in Figure 1 (space group $P2_1/c$), whereas the structures of the other compounds are compiled in the Supporting Information, Section S4. Selected bond lengths and angles of **2^R** are listed in Table 1.

The P1–C1 bonds (between 1.776(2) and 1.800(2) Å) in **2^R** are elongated by about 10 pm compared to the α-functional-
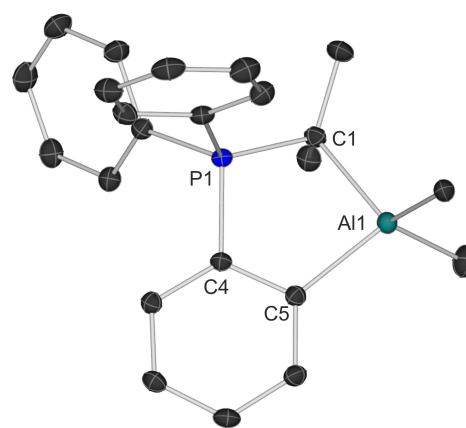

Figure 1. Molecular structures of **2^{Me}** in the solid state (ellipsoids with 30% probability). The hydrogen atoms are omitted for clarity. For selected bond lengths (Å) and angles (°), see Table 1.

Table 1. Selected bond lengths d (Å) and angles (°) of **2^R**.

	d(P1–C1)	d(C1–Al1)	d(C5–Al1)	∠(P1–C1–Al1)	$\Phi^{[a]}$
2^{Me}	1.7843(13)	2.0879(13)	2.0284(13)	103.36(6)	29.8
2^{Et}	1.776(2)	2.112(3)	2.035(3)	99.72(10)	40.0
2$^{tBu [b]}$	1.800(2)	2.118(2)	2.019(2)	102.97(10)	27.0
2^{Mes}	1.7917(12)	2.1429(12)	2.0363(11)	103.47(5)	26.8
2^{C6F5}	1.786(2)	2.050(2)	1.988(2)	101.51(9)	31.6

[a] Φ = tilt angle of the CMe$_2$ fragment at C1, i.e. the measured angle between the planes spanned by the atoms Al1, C5, C4, P1 and Al1, C1, P1; [b] reported in ref. [15].

Chemistry–A European Journal   Research Article
doi.org/10.1002/chem.202303380

Chemistry
Europe
European Chemical
Societies Publishing

ized ylides Ph₃PC(Me)BEt₂ (1.717(3) Å) or Ph₃PC(R¹)ER²₂Cl (E = Si, Ge with 1.682(2)–1.7055(15) Å) indicating a lower double bond character in this bond.[14b,c] Comparing these with the average bond lengths for P–C single (1.87 Å) and P=C double bonds (1.67 Å), the P1–C1 bonds are closer to the value for a single bond.[17] This is confirmed by the calculation of the corresponding Wiberg Bond Indices (WBI), which are close to one (0.99 and 0.97, computed for 2^{Me} and 2^{tBu}, respectively). This observation is not surprising with regard to the Lewis-acidic character of the Al fragments. The observed C1–Al1 distances (2.112(3)–2.1429(12) Å), between the Lewis-basic carbon atom and the Lewis-acidic aluminum atom, and the shorter C5–Al1 distances of 1.988(2)–2.0363(11) Å to the bridging phenylene ring, further support the findings. The P1–C1–Al1 angles of 99.64(8)–103.47(5)° slightly deviate from the ideal tetrahedral angle of 109.4°. The ylidic CMe₂ fragment at C1 is tilted by $\Phi = 26.8$–40.0° from the plane spanned by the atoms Al1, C5, C4, and P1. Overall, the crystal structures clearly show that the closed five-membered ring forms of the title compounds 2^R are the dominant resonance structures in the solid state.

Now it was of interest whether the o-AlCPs react as so-called "hidden FLPs" under ring opening with small molecules, or whether the intramolecular saturation leads to the complete cancellation of the ambiphilic character. Uhl and Lammertsma reported that the dimeric [t-Bu(H)C=C(AlEt₂)(PPhEt)]₂ (Scheme 1, top) reacts as a hidden FLP with CO₂ and PhNCO by opening the dimer to the respective adducts of the monomer.[13b] The reaction of 2^R with CO₂ allowed the isolation of the CO₂ adducts of the o-AlCPs (R=Me (3^{Me}), Et (3^{Et}), t-Bu (3^{tBu}), Mes (3^{Mes}) and C₆F₅ (3^{C6F5})) (Scheme 3). To this end, solutions of 2^R in benzene were gassed with CO₂ (1.1 bar) and then heated to 90 °C for 4–17 days. The course of the reaction was monitored by ³¹P NMR spectroscopy. When 4 bars of CO₂ were applied, the reactions were completed after 4 days at 60 °C.

Crystals of 3^{Me} and 3^{Mes}, studied by X-ray structural analysis, formed directly from the benzene solution after cooling the reaction solution to room temperature (for 3^{Me}: Figure 2; space group $P2_1/n$). 3^{Et} and 3^{tBu} crystallize by slow concentration of their benzene solutions (for 3^{tBu}: Supporting Information, Figure S52). Unfortunately, no complete data set could be obtained for the crystals of 3^{Et} and 3^{Mes}.

As can be seen from the molecular structures of 3^{Me} and 3^{tBu} in the solid state (Figure 2; Figure S52), a CO₂ molecule is inserted into the bond between the ylidic carbon atom and the aluminum fragment. The P1–C1 distance of 1.8593(13) Å in 3^{tBu} is elongated by almost 6 pm as compared to 2^{tBu} and is now very close to the value for a P–C single bond (1.87 Å) based on the atomic radii.[17] This can also be found in the P1–C1 distance (1.869(3) Å) in 3^{Me}. The angles O1–Al1–C5 = 107.08(11)° and C24–C1–P1 = 108.47(16)° for 3^{Me} and O1–Al1–C5 = 104.20(6) and C30–C1–P1 = 111.54(10) for 3^{tBu}, respectively, show an almost ideal tetrahedral coordination environment at the ylidic carbon and aluminum atoms. Comparing the angles C4–C5–Al1 (132.0(2)°) and C5–C4–P1 (119.1(2)°) in 3^{Me} and C4–C5–Al1 (132.55(11)°) and C5–C4–P1 (120.53(11)°) in 3^{tBu}, a clear widening (12°) of the angle between the bridging phenyl group and the aluminum atom can be seen. The respective Al1–O1

distances of 1.799(2) Å and 1.8075(12) Å, however, are almost identical and about 6 pm shorter than those in the CO₂ adduct of the geminal FLP published by Uhl et al.[18] By comparing the carbon–oxygen distances of O1–C24 = 1.286(3) Å and O2–C24 = 1.212(3) Å in 3^{Me} with the values for a C–O single (1.43 Å) and C=O double bond (1.19 Å), it becomes clear that the O2–C24 bond can be regarded as a slightly elongated double bond (computed WBIs of 1.66 and 1,68, for 3^{Me} and 3^{tBu}, respectively). The relatively short O1–C24 bond (WBIs of 1.19 and 1.16, respectively) indicates that the initial C=O double character in CO₂ is significantly reduced in the adduct, as expected. The corresponding bonds in 3^{tBu} show an almost identical picture. In the adducts published by Uhl and Lammertsma, the same trend can be seen.[13b,18]

The investigation in solution by ³¹P NMR spectroscopy showed a high-field shift of the signals by 3–5 ppm (Table 2). This contrasts with the lengthening of the P1–C1 distances, for which a low-field shift would be expected due to the lower double bond character. The coordination of an oxygen atom to the aluminum atom reduces its electron-withdrawing character
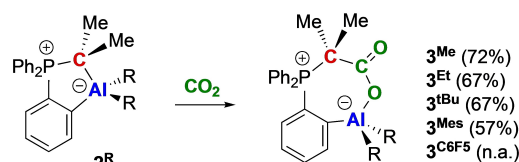
Scheme 3. Reactions of 2^R with CO₂ (4 bar) in toluene/benzene and 60 °C.

3^{Me} (72%)
3^{Et} (67%)
3^{tBu} (67%)
3^{Mes} (57%)
3^{C6F5} (n.a.)
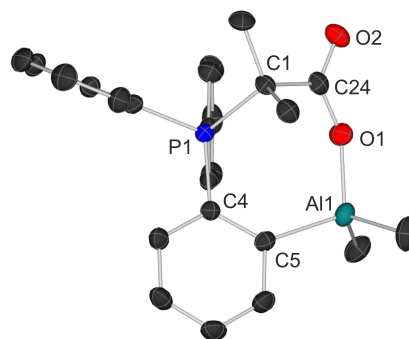
Figure 2. Molecular structure of 3^{Me} in the solid state (ellipsoids with 30% probability). The hydrogen atoms are omitted for clarity. Selected bond lengths (Å) and angles (°): P1–C1: 1.869(3), C1–C24: 1.553(4), Al1–C5: 2.012(3), Al1–O1: 1.799(2), O1–C24: 1.286(3), O2–C24: 1.212(3); O1–Al1–C5: 107.08(11), C24–C1–P1: 108.47(16), C4–C5–Al1: 132.0(2), C5–C4–P1: 119.1(2).

Table 2. ³¹P NMR chemical shifts of 2^R compared to the CO₂ adducts 3^R (ppm). Measured ν(C=O) IR stretching frequencies of 3^R (cm⁻¹).

R	$\delta_{31P}(2^R)$	$\delta_{31P}(3^R)$	ν(C=O)
Me	34.2	30.4	1657
Et	33.8	30.7	1683
t-Bu	35.4	32.5	1673
Mes	35.6	33.3	1682
C₆F₅	35.0	27.3	1677

Chemistry–A European Journal

Research Article
doi.org/10.1002/chem.202303380

Chemistry Europe
European Chemical
Societies Publishing

towards the bridging phenyl ring. The latter can thus provide more electron density for the phosphorus atom, which would explain the observed shift to the high-field.

To further substantiate the adduct formation o-AlCPs with CO_2, especially of those where no crystals could be obtained, IR spectra of the isolated compounds 3^R were measured. The observed bands associated with the $\nu(C=O)$ stretching of 3^R are similar in all cases and appear in the usual range for C=O double bonds (see Table 2).

Moreover, the formation of the CO_2 adducts 3^R has been also studied computationally by means of Density Functional 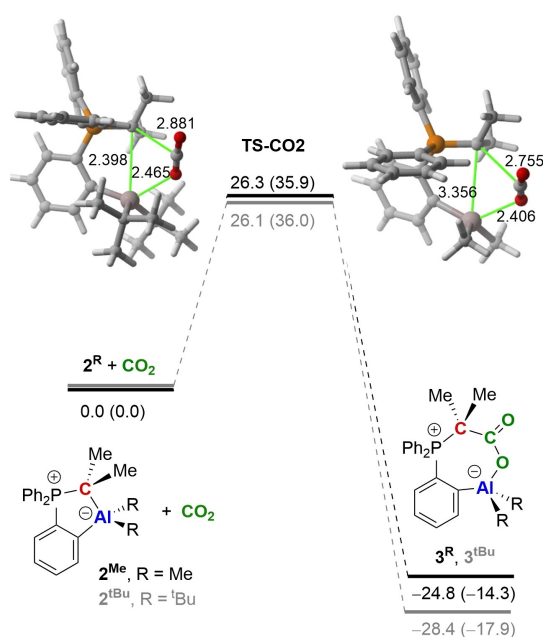Theory (DFT) calculations at the PCM(benzene)-B3LYP-D3/def2-SVP level (see computational details in the Supporting Information, section S5). As depicted in Figure 3, which shows the computed reaction profiles for the reactions involving 2^{Me} and 2^{tBu}, the process occurs in a concerted manner leading to the formation of the new (P)C–C(=O) and Al–O(CO) bonds with concomitant rupture of the initial Al–C(P) bond in 2^R.[22] The process is exergonic by ΔG_R of approx. −14 to −18 kcal/mol, which is in agreement with the observed stability of the CO_2 adducts under our conditions. In addition, the computed activation barriers of $\Delta G^{\neq} \approx 36$ kcal/mol are consistent with the observed low reaction rates at 90 °C (4–17 days). This CO_2 activation is therefore rather different from the analogous process involving the reversible, stepwise activation of NH_3.[15]

Similar to related intramolecular FLPs,[19] the cooperative action of the Lewis antagonists in 2^R can be revealed by applying the Natural Orbital for Chemical Valence (NOCV) method. As shown in Figure 4, the NOCV method indicates that two different orbital interactions take place simultaneously during the CO_2 activation mediated by 2^R, namely the donation from the ylide to the $\pi^*(C=O)$ molecular orbital (denoted as $\rho 1$) and the donation from the terminal oxygen atom of the CO_2 to the vacant p-atomic orbital of the aluminum atom (denoted as $\rho 2$). According to the associated stabilization energies ($\Delta E(\rho)$) computed for the transition state involved in the $2^{Me} + CO_2$ reaction, $\rho 1$ is stronger than $\rho 2$, which resembles the mode of action of related FLPs in the activation of CO_2,[19d,e] therefore confirming the reactivity likeness of these species.

Next, we turned our attention to the catalytic reduction of CO_2 with HBpin as stoichiometric reduction equivalent. In a first attempt, we subjected the CO_2 adduct 3^{tBu} to the reaction with HBpin. Neither at RT nor at 60 °C a transformation was observed (see Supporting Information, Figure S39). This observation renders 3^{tBu} as a catalytically incompetent off-cycle intermediate. However, when 2^{tBu} was mixed with 30 equiv. HBpin in benzene-d_6, degassed and subsequently exposed to 4 bar CO_2 full conversion of the borane was observed (Scheme 4).

After heating of the mixture to 60 °C for 6 days, ^{11}B NMR spectroscopy confirmed the catalytic conversion of CO_2 into boric esters. Furthermore, the metallacycle 2^{tBu} was fully regenerated as confirmed by ^1H and ^{31}P NMR spectroscopy, rendering the catalytic reduction of CO_2 most feasible.

Next, we investigated the impact of the R group in 2^R on the catalytic reduction of CO_2 with HBpin. Solutions of 2^R and 30 equiv. of HBpin in 0.6 ml benzene-d_6 were prepared, providing a 0.57 M solution with respect to HBpin and 3 mol% of catalyst. The reaction mixtures were degassed and subsequently exposed to 4 bar CO_2, sealed and then heated to 60 °C. The formation of MeOBpin was monitored over a period

Figure 3. Computed profile for the reaction of CO_2 with 2^{Me} (black lines) and 2^{tBu} (grey lines). Relative energies (free energies, computed at 298 K, within parentheses) and bond distances in the transition states **TS-CO2** are given in kcal/mol and angstroms, respectively. All data have been computed at the PCM(benzene)-B3LYP-D3/def2-SVP level.

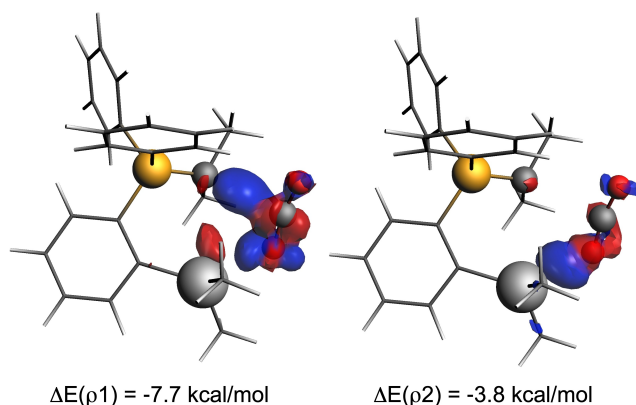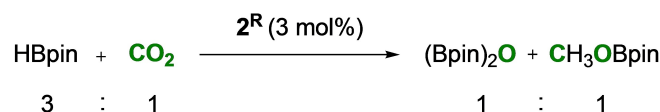$\Delta E(\rho 1) = -7.7$ kcal/mol $\Delta E(\rho 2) = -3.8$ kcal/mol

Figure 4. Contour plots of NOCV deformation densities $\Delta\rho$ (isovalue of 0.001 a.u.) and associated energies $\Delta E(\rho)$ for the main orbital interactions between CO_2 and 2^{Me} in the corresponding transition state. Electronic charge flows from red to blue. All data were computed at the ZORA-B3LYP-D3/TZ2P//PCM(benzene)-B3LYP-D3/def2-SVP level.

Scheme 4. Catalytic reduction of CO_2 (4 bar) with HBpin in benzene-d_6 at 60 °C.

Chemistry–A European Journal

Research Article
doi.org/10.1002/chem.202303380

Chemistry Europe
European Chemical
Societies Publishing

of 6 days by ^1H NMR spectroscopy using C_6Me_6 as internal standard.

The reaction profiles in Figure 5 show that the *t*-Bu derivative **2^tBu** (black datapoints) is the most efficient one and provides quantitative conversion of HBpin into MeOBpin.

Conversion with **2^Mes** (yellow datapoints) reached 58% after 6 days at 60°C, whereas **2^Me** (blue) and **2^Et** (orange) reached a plateau at 52% (after three days) and 43% (after one day), respectively (details in Supporting Information Table S2). Qualitatively, the reaction profiles of **2^tBu**, **2^Mes** and **2^C6F5** show almost linear behaviour up to 60% conversion. For **2^C6F5** (violet-blue) only slow formation of MeOBpin is observed, but even after 6 days a decrease of the catalyst's performance is not noted. This is in stark contrast to **2^Me** and **2^Et**, which are deactivated after 40–50% conversion is reached. During these reactions, colorless precipitates were formed, which most likely corre-
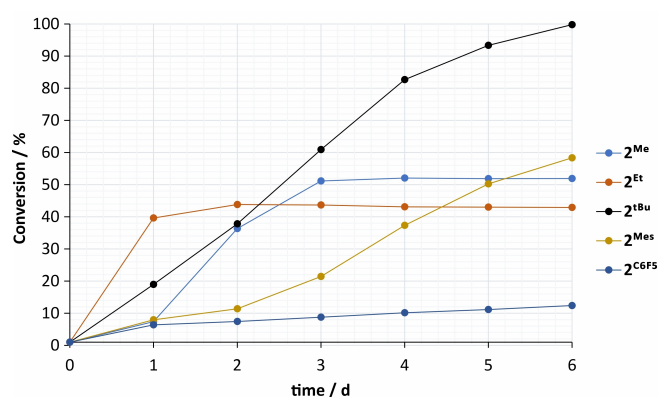
spond to the respective CO_2 adducts of **3^Me** and **3^Et**. These species are insoluble in benzene and do not react with HBpin at 60°C, so that they are removed from the catalytic cycle. This finding is in full support of your initial experiment with **3^tBu**/HBpin (vide supra) and is fully supported by our computational experiments (compare Figure 3 and Figure 6).

The catalyzed reaction of **2^tBu** was stopped by the addition of water and subjected to NMR spectroscopy. A yield of 68% of MeOH was determined by ^1H NMR spectroscopy using C_6Me_6 as internal standard (Figure S42 in the Supporting Information). While the kinetic data presented in Figure 5 should be approached with caution, it is possible to make a careful comparison of catalytic performance with reported related systems. The TOFs of the Al-based catalysts **2^R** vary between 0.03–0.27 h^{-1} (see Supporting Information, Table S2), which falls into the range of the square-planar Al complexes reported by Greb (TOF = 0.12 h^{-1}) and Riddlestone (TOF = 0.08).[20] Related group 2 and aluminum hydride complexes, which undergo hydrometallation in the CO_2 reduction, show comparable TOFs of 0.07–0.16 h^{-1}.[5a,21]

To shed light on the mechanism of the catalytic reduction of CO_2 by HBpin mediated by **2^R**, DFT calculations were conducted on the system involving **2^Me** as a representative example and using a model borane where the methyl groups in HBpin were replaced by hydrogen atoms (HBeg). As can be seen from the computed reaction profile provided in Figure 6, the process begins with the insertion of one B—O entity of the borane into the Al—C bond of **2^Me** through transition state **TS1** ($\Delta G^{\neq} = 32.1$ kcal/mol) thus forming **INT1**. This reaction is kinetically favored over the alternative B—H activation reaction, which according to its computed barrier ($\Delta G^{\neq} = 40.0$ kcal/mol) seems unfeasible, and over the initial CO_2 activation ($\Delta G^{\neq} = 35.9$ kcal/mol, see Figure 3). Subsequent exergonic ($\Delta G = -10.1$ kcal/mol)

Figure 5. Kinetic studies of the catalytic reduction of CO_2 with HBpin and 3.3 mol% **2^R**. Plotted is the conversion of HBpin vs. reaction time. Catalyst concentration of 10 mol% (3.33 mol%) based on CO_2 (HBpin).

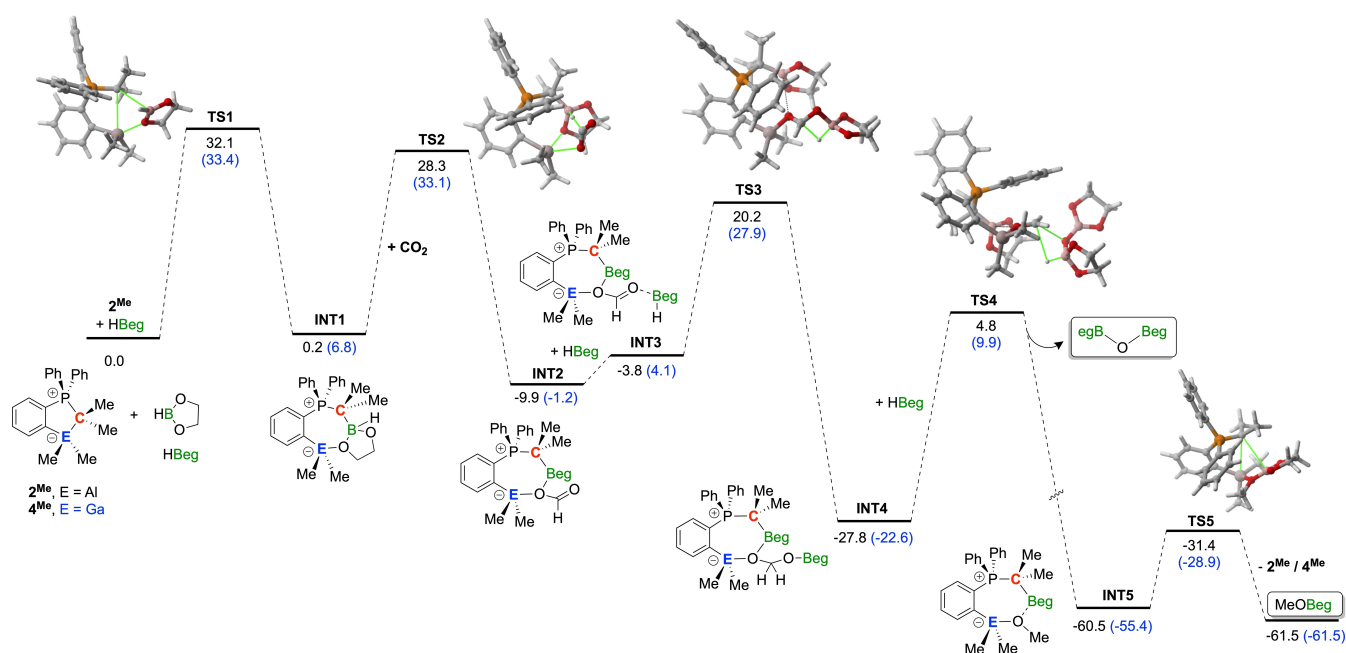**Figure 6.** Computed reaction profiles of the catalytic reduction of CO_2 using model HBeg mediated by **2^Me** (black values) or **4^Me** (blue values). Relative free energies (ΔG, at 298 K) are given in kcal/mol. All data have been computed at the PCM(benzene)-B3LYP-D3/def2-SVP level.

Chem. Eur. J. **2023**, e202303380 (5 of 10)

© 2023 The Authors. Chemistry - A European Journal published by Wiley-VCH GmbH

Chemistry–A European Journal

Research Article
doi.org/10.1002/chem.202303380

Chemistry
Europe
European Chemical
Societies Publishing

activation reaction of CO_2 takes place to form **INT2**, a similar species to those reported for the process involving the above-mentioned aluminum hydrides.[5] This reaction, which exhibits an accessible barrier of 28.1 kcal/mol (from **INT1**), occurs via **TS2**, a saddle point associated with the hydride addition to the electrophilic carbon atom of CO_2 with concomitant formation of the Al–O(C=O) bond. Subsequent slightly endergonic ($\Delta G = 6.1$ kcal/mol) coordination of a second molecule of the borane produces **INT3**, which undergoes a hydroboration reaction through **TS3** ($\Delta G^{\neq} = 24.4$ kcal/mol) to afford intermediate **INT4** in a highly exothermic reaction ($\Delta G = -24$ kcal/mol). Subsequent reaction with a new molecule of borane produces **INT3** in a strongly exergonic reaction ($\Delta G = -32.7$ kcal/mol). The next reaction step takes place via **TS4**, a saddle point associated with the formation of the final C–H bond with concomitant release of (Beg)O(Beg), with a barrier of 32.6 kcal/mol. Final elimination reaction through **TS5** ($\Delta G^{\neq} = 29.1$ kcal/mol) affords the fully reduced MeOBeg molecule with concomitant regeneration of the catalytic species $\mathbf{2^{Me}}$ in a slightly exergonic transformation ($\Delta G = -1.0$ kcal/mol).

For completeness, we also computed the alternative profile starting from the CO_2-activated product $\mathbf{3^{Me}}$ (see Supporting Information Figure S56). Our calculations indicate that whereas the first hydroboration reaction is feasible ($\Delta G^{\neq} = 35.0$ kcal/mol), the second hydroboration reaction is unfeasible (barrier ca. 60 kcal/mol), which is compatible with the lack of reactivity of $\mathbf{3^{tBu}}$ observed experimentally (see above).

Having the HBpin (HBeg) activation involving the o-AlCPs and the capability of CO_2 reduction of the reported Ga hydride complexes of Aldridge and Goicoechea in mind,[22] we prepared the o-GaCPs analogues $\mathbf{4^R}$ and investigated their activity as catalysts for the reduction of CO_2.

The o-GaCPs (2-{GaR$_2$}-C$_6$H$_4$)Ph$_2$PCMe$_2$ (R=Et ($\mathbf{4^{Et}}$), t-Bu ($\mathbf{4^{tBu}}$), and C$_6$F$_5$ ($\mathbf{4^{C6F5}}$)) were prepared in the same way as the o-AlCPs (Scheme 2). Recrystallization from hexane or cyclopentane afforded $\mathbf{4^R}$ in pure form in yields of 15–59%. Crystals of all o-GaCPs $\mathbf{4^R}$ could be investigated by X-ray structure analysis. The molecular structure of $\mathbf{4^{Et}}$ in the solid state is exemplarily shown in Figure 7 (space group $P\bar{1}$). The structures of the other compounds are compiled in the Supporting Information, Section S4. Selected bond lengths and angles of $\mathbf{4^R}$ are listed in Table 3, which, as expected, are quite similar to those found in their Al counterparts $\mathbf{2^R}$.

$\mathbf{4^{tBu}}$ showed the same stability towards air and moisture as reported for $\mathbf{2^{tBu}}$.[15] It can be stored on the bench for weeks and NMR spectra can be recorded in non-dried solvents without any signs of decomposition. In contrast, $\mathbf{4^{Et}}$ decomposes slowly by

applying high vacuum, in solution, and while storing the solid in the glovebox at ambient temperature.

Although our DFT calculations suggest that the formation of the CO_2 adduct ($\Delta G^{\neq} = 32.4$ kcal/mol) starting from $\mathbf{4^R}$ is related to their aluminum derivatives $\mathbf{2^R}$, the process is much less exergonic ($\Delta G_R = -7.7$ kcal/mol for $\mathbf{4^{tBu}}$) than for the corresponding Al derivatives ($\Delta G_R = -17.9$ kcal/mol for $\mathbf{2^{tBu}}$, cf. Figure 3). Exposing of a solution of $\mathbf{4^{tBu}}$ to CO_2 (1.1 bar) and heating for a week did neither furnish the adduct, nor other reactions did occur according to the ^1H and ^{31}P NMR spectra. Despite that, we successfully applied $\mathbf{4^{tBu}}$ and $\mathbf{4^{C6F5}}$ in the catalytic reduction of CO_2 using HBpin (Table 4), which further strongly supports the insertion of the borane as the initial step in the CO_2 reduction.

$\mathbf{4^{tBu}}$ and $\mathbf{4^{C6F5}}$ showed catalytic activities that exceed that of the aluminum analogues $\mathbf{2^R}$ by an order of magnitude. Even with lower catalyst loadings of 0.3 mol% (3 mol% for Al derivatives) based on HBpin, the reaction times are significantly reduced to 24–48 h. Surprisingly, the catalytic activity of the o-GaCPs $\mathbf{4^R}$ surpass the activity of the reported Ga hydrides (TOF = 2.5 and 2.6 h^{-1}). Quenching the reaction mixture of $\mathbf{4^{tBu}}$ with H_2O gave 77% of methanol according to ^1H NMR spectroscopic investigations using C_6Me_6 as internal standard.

The significantly increased catalytic activity of the Ga derivatives compared to the Al analog may be accounted by two ways. First, the strongly exergonic off-cycle deactivation pathway involving the formation of the CO_2 adducts $\mathbf{3^R}$ is absent for the Ga derivatives, leading to a higher concentration of catalytically competent species (Scheme 5). Second, a more feasible energetic profile (Figure 6) may be present for the Ga derivatives. Indeed, our calculations confirm that the process
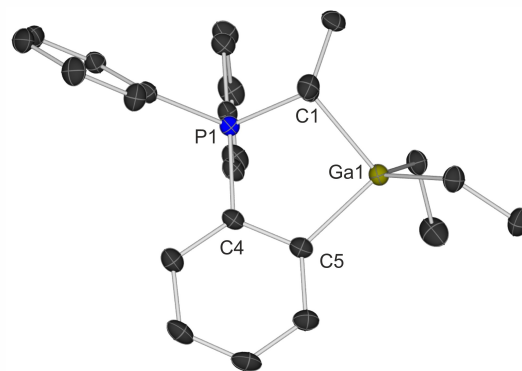
Figure 7. Molecular structure of $\mathbf{4^{Et}}$ in the solid state (ellipsoids with 30% probability). The hydrogen atoms are omitted for clarity. For selected bond lengths (Å) and angles (°), see Table 3.

Table 3. Selected bond lengths d (Å) and angles (°) of $\mathbf{4^R}$.					
	d(P1–C1)	d(C1–Ga1)	d(C5–Ga1)	$\angle$(P1–C1–Ga1)	Φ[a]
$\mathbf{4^{Et}}$	1.7748(18)	2.1155(18)	2.0285(17)	99.64(8)	37.5
$\mathbf{4^{tBu}}$	1.797(2)	2.139(2)	2.028(2)	102.47(9)	27.4
$\mathbf{4^{C6F5}}$	1.787(2)	2.069(2)	1.995(2)	100.68(10)	31.8
[a] Φ = tilt angle of the CMe$_2$ fragment at C1, i.e. the measured angle between the planes spanned by the atoms Ga1, C5, C4, P1 and Ga1, C1, P1.					

Table 4. Conversion of HBpin. Catalyst concentration of 0.3 mol% based on HBpin.

	Time/d[a]	Conversion/%[b]	TOF/h^{-1}[c]
4^{tBu}	2	98	6.11
4^{C6F5}	1	96	12.00

[a] Time where no more reaction was observed; [b] referred to C_6Me_6 as internal standard; [c] determined after no further conversion was observed.
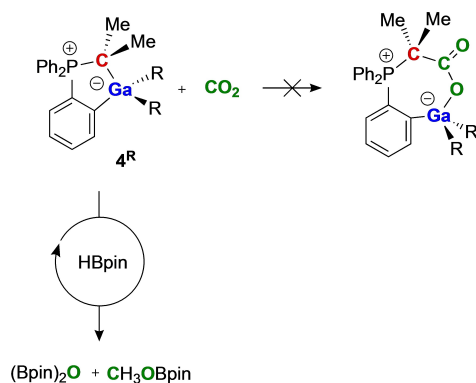
Scheme 5. Pathways of the reaction between **4^R**, CO_2 and HBpin.

involving **4^{Me}** proceeds through a rather similar reaction pathway where the final elimination step, leading to the fully reduced MeOBpin (MeOBeg in the calculations) and **4^{Me}**, is more exergonic ($\Delta G = -6.2$ kcal/mol) and requires a lower activation barrier ($\Delta G^{\neq} = 26.4$ kcal/mol, see Figure 6).

Conclusions

We report on a rare combination of an aluminum or gallium Lewis acid and a carbon Lewis base in the field of frustrated Lewis pair chemistry. Herein, we further elaborate on a new class of hidden FLPs consisting of a phosphorus ylide featuring an aluminum or gallium fragment in the *ortho* position of a phenyl ring scaffold. The *o*-AlCPs (**2^R**) and *o*-GaCPs (**4^R**) are accessible through salt metathesis of the lithiated ylide **1** with the corresponding dialkyl element halides. Although the formation of the intramolecular Lewis acid/base adduct was observed in the solid state, the *o*-AlCPs (**2^R**) readily react with carbon dioxide (CO_2), forming stable adducts **3^R**. The analogous gallium derivatives **4^R**, however, were surprisingly unreactive towards CO_2. Despite this, all title compounds are capable of catalyzing the reduction of CO_2 to methanol with satisfactory high selectivity, yields, and low catalyst loadings of 0.3–3 mol% using HBpin as stoichiometric reduction equivalent. The computed reaction profile suggests that the reduction is initiated by the insertion of one B–O entity of the borane into the E–C bond (E=Al, Ga) followed by the hydride addition to CO_2 and *not* by the adduct formation with CO_2. Interestingly, *o*-GaCPs **4^{tBu}** and **4^{C6F5}** exceed the *o*-AlCPs **2^R** in orders of magnitude in their catalytic activity. It is assumed that the

suppressed reaction pathway of the CO_2 adduct formation, on the one hand, leads to full conversion in both cases with **4^R**, and on the other hand, makes the reduction of CO_2 more favorable.

Experimental Section

General Methods: All operations were carried out under dry argon using standard Schlenk and glovebox techniques. *t*-BuLi (1.7 M in pentane), Me$_2$AlCl, Et$_2$AlCl, and ZnMe$_2$ (1 M toluene) were used as purchased from Sigma–Aldrich. The ylide Ph$_3$PCMe$_2$,[23] *t*-Bu$_2$AlCl,[24] (C$_6$F$_5$)$_2$Zn,[25] Et$_2$GaCl[26] and *t*-Bu$_2$GaCl[27] were synthesized according to literature procedures. Solvents were dried over Na/K or CaH$_2$ and rigorously degassed before use. NMR spectra were recorded on a Bruker Avance Neo 400 or an Avance 300 spectrometer operating at ^{1}H Larmor frequencies of 400 or 300 MHz in dry degassed deuterated solvents. For the kinetic studies we used a Migratek Spinsolve 80 Benchtop NMR spectrometer. ^{1}H, and ^{13}C{^{1}H} chemical shifts where reported against TMS, ^{31}P{^{1}H} against H$_3$PO$_4$ and ^{19}F against BF$_3$OEt$_2$. Coupling constants (*J*) are given in Hertz as positive values, regardless of their real individual signs. IR spectra were measured on a Bruker Alpha spectrometer using the attenuated reflection technique (ATR) and the data are quoted in wavenumbers (cm^{-1}). Melting points were measured with a Thermo Fischer melting point apparatus and are not corrected. Elemental analyses were carried out in the institutional technical laboratories of the Karlsruhe Institute of Technology (KIT).

General protocol for the synthesis of the compounds 2^R and 4^R: In a vial in a glovebox, **1** is suspended in toluene and 1 equiv. of R$_2$AlX (X=Cl, Br) or R$_2$GaCl, either pure or in solution, is added. After stirring for a certain period of time, the reaction mixture is filtered, the resulting solution is concentrated and the products are isolated by crystallization. See Supporting Information for details.

2^{Me} (147 mg, 25%) colorless platelets. M.p. (decomp.): 136°C. ^{1}H NMR (300 MHz, 298 K, C$_6$D$_6$, ppm): $\delta = 8.25$–8.23 (m, H$_{PhAl\_ortho}$, 1H), 7.38–7.31 (m, H$_{Arr}$, 4H), 7.31–7.29 (m, H$_{PhAl\_para}$, 1H), 7.08–6.96 (m, H$_{Ph2\_meta}$, 4H), 6.96–6.85 (m, H$_{Ph2\_otho}$, 4H), 1.48 (d, $^3J_{PH} = 20.7$ Hz, H$_{CMe2}$, 6H), −0.31 (s, H$_{AlMe2}$, 6H). ^{13}C{^{1}H} NMR (75 MHz, 298 K, C$_6$D$_6$, ppm): $\delta = 138.3$ (d, $^2J_{PC} = 20.5$ Hz, C$_{PhAl\_ortho}$), 134.4 (d, $^4J_{PC} = 8.5$ Hz, C$_{PPh2\_para}$), 132.0 (d, $^4J_{PC} = 2.8$ Hz, C$_{PhAl\_para}$), 131.9 (d, $^3J_{PC} = 2.9$ Hz, C$_{PhAl\_meta}$), 131.7 (d, $^2J_{PC} = 14.0$ Hz, C$_{PPh2\_ortho}$), 131.6 (d, $^1J_{PC} = 99.2$ Hz, C$_{PPh2\_ipso}$), 128.7 (d, $^3J_{PC} = 10.6$ Hz, C$_{PPh2\_meta}$), 127.1 (d, $^3J_{PC} = 12.5$ Hz, C$_{PhAl\_meta}$), 124.5 (d, $^1J_{PC} = 67.4$ Hz, C$_{CMe2}$), 21.5 (d, $^2J_{PC} = 2.5$ Hz, C$_{CMe2}$), −9.5 (s, C$_{AlMe2}$). ^{31}P{^{1}H} NMR (121 MHz, 298 K, C$_6$D$_6$, ppm): $\delta = 34.2$ (s). IR (ATR, cm^{-1}): see the Supporting Information. Elemental analysis (%): (calcd., found for C$_{23}$H$_{26}$AlP; C (76.65, 76.97), H (7.27, 7.19).

2^{Et} colorless solid (412 mg, 66%). M.p. (decomp.): 85°C. ^{1}H NMR (300 MHz, 298 K, C$_6$D$_6$, ppm): $\delta = 8.30$–8.23 (m, H$_{PhAl\_ortho}$, 1H), 7.38–7.34 (m, H$_{PhAl\_meta}$, 1H), 7.34–7.32 (m, H$_{PhAl\_meta}$, 1H), 7.32–7.29 (m, H$_{Ph2\_para}$, 2H), 7.29–7.26 (m, H$_{PhAl\_para}$, 1H), 7.08–6.95 (m, H$_{Ph2\_meta}$, 4H), 6.95–6.86 (m, H$_{Ph2\_otho}$, 4H), 1.61 (t, $^3J_{HH} = 8.0$ Hz, H$_{AlCH2CH3}$, 6H), 1.50 (d, $^3J_{PH} = 20.9$ Hz, H$_{CMe2}$, 6H), 0.45–0.17 (m, H$_{AlCH2CH3}$, 4H). ^{13}C{^{1}H} NMR (75 MHz, 298 K, C$_6$D$_6$, ppm): $\delta = 138.7$ (d, $^2J_{PC} = 20.5$ Hz, C$_{PhAl\_ortho}$), 134.4 (d, $^4J_{PC} = 7.9$ Hz, C$_{PPh2\_para}$) 132.0 (d, $^2J_{PC} = 15.4$ Hz, C$_{PPh2\_ortho}$), 132.0 (d, $^4J_{PC} = 2.9$ Hz, C$_{PhAl\_para}$), 132.3 (d, $^1J_{PC} = 104.7$ Hz, C$_{PPh2\_ipso}$), 131.2 (d, $^3J_{PC} = 3.6$ Hz, C$_{PhAl\_meta}$), 128.7 (d, $^3J_{PC} = 10.6$ Hz, C$_{PPh2\_meta}$), 127.6 (d, $^3J_{PC} = 12.4$ Hz, C$_{PhAl\_meta}$), 124.4 (d, $^1J_{PC} = 67.4$ Hz, C$_{CMe2}$), 21.6 (d, $^2J_{PC} = 2.6$ Hz, C$_{CMe2}$), 11.3 (s, C$_{AlCH2CH3}$), 0.7 (bs, C$_{AlCH2CH3}$). ^{31}P{^{1}H} NMR (121 MHz, 298 K, C$_6$D$_6$, ppm): $\delta = 33.8$ (s). IR (ATR, cm^{-1}): see the Supporting Information. Elemental analysis (%): (calcd., found for C$_{25}$H$_{30}$AlP·0.5Tol); C (78.77, 78.66), H (7.89, 7.49).

Chemistry–A European Journal

Research Article
doi.org/10.1002/chem.202303380

Chemistry Europe
European Chemical
Societies Publishing

2^{Mes} (79 mg, 28%) colorless crystals. M.p. (decomp.): 215 °C. ^{1}H NMR (400 MHz, 298 K, C$_6$D$_6$, ppm): $\delta = 8.35$–8.32 (m, H$_{PhAl\_ortho}$, 1H), 7.40–7.37 (m, H$_{PhAl\_meta}$, 1H), 7.35–7.34 (m, H$_{PhAl\_meta}$, 1H), 7.33–7.31 (m, H$_{Ph2\_para}$, 2H), 7.31–7.20 (m, H$_{PhAl\_para}$, 1H), 7.03–6.95 (m, H$_{Ph2\_meta}$, 4H), 6.85–6.84 (m, H$_{Mes\_meta}$, 4H) 6.84–6.80 (m, H$_{Ph2\_otho}$, 4H), 2.50 (s, H$_{Mes\_ortho}$, 12H), 2.28 (s, H$_{Mes\_para}$, 6H), 1.63 (d, $^3J_{PH} = 21.0$ Hz, H$_{CMe2}$, 6H). ^{13}C{^{1}H} NMR (75 MHz, 298 K, C$_6$D$_6$, ppm): $\delta = 145.2$ (s, C$_{Mes\_ipso}$), 140.1 (d, $^2J_{PC} = 19.3$ Hz, C$_{PhAl\_ortho}$), 135.1 (s, C$_{Mes\_para}$), 134.9 (d, $^4J_{PC} = 7.8$ Hz, C$_{PPh2\_para}$) 132, 4 (d, $^2J_{PC} = 13.7$ Hz, C$_{PPh2\_ortho}$), 132.2 (d, $^4J_{PC} = 2.7$ Hz, C$_{PhAl\_para}$), 131.7 (d, $^3J_{PC} = 4.0$ Hz, C$_{PhAl\_meta}$), 129.9 (d, $^1J_{PC} = 100.4$ Hz, C$_{PPh2\_ipso}$), 128.8 (d, $^3J_{PC} = 10.1$ Hz, C$_{PPh2\_meta}$), 127.4 (s, C$_{Mes\_meta}$) 127.0 (d, $^3J_{PC} = 12.2$ Hz, C$_{PhAl\_meta}$), 125.7 (s, C$_{Mes\_ortho}$), 124.1 (d, $^1J_{PC} = 68.0$ Hz, C$_{CMe2}$), 26.7 (s, C$_{Me\_ortho}$), 23.7 (d, $^2J_{PC} = 3.8$ Hz, C$_{CMe2}$), 21.3 (s, C$_{Me\_para}$). ^{31}P{^{1}H} NMR (121 MHz, 298 K, C$_6$D$_6$, ppm): $\delta = 35.6$ (s). IR (ATR, cm^{-1}): see the Supporting Information. Elemental analysis (%): (calcd., found for C$_{39}$H$_{42}$AlP); C (82.37, 82.39), H (7.44, 7.16).

2^{C6F5} (85 mg, 34%) colorless solid. M.p. (decomp.): 96 °C. ^{1}H NMR (300 MHz, 298 K, C$_6$D$_6$, ppm): $\delta = 8.77$–8.70 (m, H$_{PhAl\_ortho}$, 1H), 7.45–7.35 (m, H$_{PhAl\_meta}$, H$_{PhAl\_meta}$, 2H), 7.24–7.21 (m, H$_{Ph2\_para}$, 2H), 7.20–7.19 (m, H$_{PhAl\_para}$, 1H), 7.10–6.97 (m, H$_{Ph2\_meta}$, H$_{Ph2\_otho}$, 8H), 1.49 (d, $^3J_{PH} = 20.6$ Hz, H$_{CMe2}$, 6H). ^{13}C{^{1}H} NMR (75 MHz, 298 K, C$_6$D$_6$, ppm): $\delta = 138.7$ (d, $^2J_{PC} = 18.9$ Hz, C$_{PhAl\_ortho}$), 134.4 (d, $^4J_{PC} = 8.2$ Hz, C$_{PPh2\_para}$) 133.6 (d, $^2J_{PC} = 9.5$ Hz, C$_{PPh2\_ortho}$), 132.8 (d, $^4J_{PC} = 2.9$ Hz, C$_{PhAl\_para}$), 132.4 (d, $^3J_{PC} = 3.7$ Hz, C$_{PhAl\_meta}$), 130.9 (d, $^1J_{PC} = 103.1$ Hz, C$_{PPh2\_ipso}$), 128.5 (d, $^3J_{PC} = 11.3$ Hz, C$_{PPh2\_meta}$), 128.8 (d, $^3J_{PC} = 10.8$ Hz, C$_{PhAl\_meta}$), 121.7 (d, $^1J_{PC} = 72.1$ Hz, C$_{CMe2}$), 20.4 (m, C$_{CMe2}$). ^{31}P{^{1}H} NMR (121 MHz, 298 K, C$_6$D$_6$, ppm): $\delta = 35.0$ (s). ^{19}F NMR (282 MHz, 298 K, C$_6$D$_6$, ppm): $\delta = -119.1$ (m, C$_6$F$_{5\_meta}$), -155.2 (t, $^2J_{FF} = 19.6$ Hz C$_6$F$_{5\_ortho}$), -162.0 (m, C$_6$F$_{5\_para}$). IR (ATR, cm^{-1}): see the Supporting Information. Elemental analysis: Due to the high fluorine content no satisfactory elemental analysis could be obtained.

4^{Et} (150 mg, 15%) colorless crystals. M.p.: 84 °C. ^{1}H NMR (300 MHz, 298 K, C$_6$D$_6$, ppm): $\delta = 8.26$ - 8.20 (m, H$_{PhGa\_ortho}$, 1H), 7.38–7.32 (m, H$_{PhGa\_meta}$, 2H), 7.32–7.29 (m, H$_{Ph2\_para}$, 2H), 7.26–7.26 (m, H$_{PhGa\_para}$, 1H), 7.07–6.96 (m, H$_{Ph2\_meta}$, 4H), 6.96–6.86 (m, H$_{Ph2\_otho}$, 4H), 1.62 (t, $^3J_{HH} = 8.0$ Hz, H$_{GaCH2CH3}$, 6H), 1.55 (d, $^3J_{PH} = 20.3$ Hz, H$_{CMe2}$, 6H), 0.76–0.46 (m, H$_{GaCH2CH3}$, 4H). ^{13}C{^{1}H} NMR (75 MHz, 298 K, C$_6$D$_6$, ppm): $\delta = 138.3$ (d, $^2J_{PC} = 19.4$ Hz, C$_{PhGa\_ortho}$), 134.4 (d, $^4J_{PC} = 7.8$ Hz, C$_{PPh2\_para}$) 132.2 (d, $^2J_{PC} = 16.1$ Hz, C$_{PPh2\_ortho}$), 131.9 (d, $^4J_{PC} = 2.8$ Hz, C$_{PhGa\_para}$), 131.6 (d, $^1J_{PC} = 107.8$ Hz, C$_{PPh2\_ipso}$), 131.1 (d, $^3J_{PC} = 3.6$ Hz, C$_{PhGa\_meta}$), 128.6 (d, $^3J_{PC} = 10.6$ Hz, C$_{PPh2\_meta}$), 126.5 (d, $^3J_{PC} = 12.5$ Hz, C$_{PhGa\_meta}$), 124.7 (d, $^1J_{PC} = 67.6$ Hz, C$_{CMe2}$), 22.2 (d, $^2J_{PC} = 1.3$ Hz, C$_{CMe2}$), 12.6 (s, C$_{GaCH2CH3}$), 2.5 (bs, C$_{GaCH2CH3}$). ^{31}P{^{1}H} NMR (121 MHz, 298 K, C$_6$D$_6$, ppm): $\delta = 34.4$ (s). IR (ATR, cm^{-1}): see the Supporting Information. Elemental analysis (%): Due to the high sensitivity towards air and moisture no satisfactory elemental analysis could be obtained.

4^{tBu} (318 mg, 59%) colorless solid. M.p.: 148 °C. ^{1}H NMR (300 MHz, 298 K, C$_6$D$_6$, ppm): $\delta = 8.23$–8.18 (m, H$_{PhAl\_ortho}$, 1H), 7.33–7.30 (m, H$_{PhAl\_meta}$, 2H), 7.30–7.26 (m, H$_{Ph2\_para}$, 2H), 7.26–7.23 (m, H$_{PhAl\_para}$, 1H), 7.00–6.88 (m, H$_{Ph2\_meta}$, 4H), 6.87–6.77 (m, H$_{Ph2\_otho}$, 4H), 1.63 (d, $^3J_{PH} = 21.4$ Hz, H$_{CMe2}$, 6H), 1.32 (s, H$_{CMe3}$, 18H). ^{13}C{^{1}H} NMR (75 MHz, 298 K, C$_6$D$_6$, ppm): $\delta = 174.9$ (d, $^1J_{PC} = 35.6$ Hz, C$_{PhGa\_ipso}$), 138.9 (d, $^2J_{PC} = 19.9$ Hz, C$_{PhGa\_ortho}$), 134.6 (d, $^4J_{PC} = 7.5$ Hz, C$_{PPh2\_para}$), 133, 4 (d, $^2J_{PC} = 14.9$ Hz, C$_{PPh2\_ortho}$), 131.9 (d, $^4J_{PC} = 2.8$ Hz, C$_{PhGa\_para}$), 130.9 (d, $^1J_{PC} = 108.6$ Hz, C$_{PPh2\_ipso}$), 131.1 (d, $^3J_{PC} = 3.6$ Hz, C$_{PhGa\_meta}$), 128.6 (d, $^3J_{PC} = 10.5$ Hz, C$_{PPh2\_meta}$), 126.2 (d, $^3J_{PC} = 12.1$ Hz, C$_{PhGa\_meta}$), 124.9 (d, $^1J_{PC} = 65, 9$ Hz, C$_{CMe2}$), 33.8 (s, C$_{CMe3}$), 25.4 (d, $^2J_{PC} = 2.37$ Hz, C$_{CMe2}$), 23.4 (s, C$_{CMe3}$), 19.1 (d, $^2J_{PC} = 19.1$ Hz, C$_{PhGa\_ortho}$). ^{31}P{^{1}H} NMR (121 MHz, 298 K, C$_6$D$_6$, ppm): $\delta = 36.4$ (s). IR (ATR, cm^{-1}): see the Supporting Information. Elemental analysis (%): (calcd., found for C$_{29}$H$_{38}$GaP·0.5Tol); C (73.18, 72.93), H (7.94, 7.63).

4^{C6F5} (119 mg, 18%) colorless crystals. M.p.: 183 °C. ^{1}H NMR (300 MHz, 298 K, C$_6$D$_6$, ppm): $\delta = 8.74$–8.69 (m, H$_{PhAl\_ortho}$, 1H), 7.45–7.38 (m, H$_{PhAl\_meta}$, H$_{PhAl\_meta}$, 2H), 7.15–7.10 (m, H$_{Ph2\_para}$, 2H), 7.04–

6.98 (m, H$_{PhAl\_para}$, 1H), 6.96–6.73 (m, H$_{Ph2\_meta}$, H$_{Ph2\_ortho}$, 8H), 1.52 (d, $^3J_{PH} = 19.9$ Hz, H$_{CMe2}$, 6H). ^{13}C{^{1}H} NMR (75 MHz, 298 K, C$_6$D$_6$, ppm): $\delta = 139.5$ (d, $^2J_{PC} = 15.6$ Hz, C$_{PhAl\_ortho}$), 134.4 (d, $^4J_{PC} = 8.3$ Hz, C$_{PPh2\_para}$) 133.6 (d, $^2J_{PC} = 9.5$ Hz, C$_{PPh2\_ortho}$), 132.8 (m, $^4J_{PC}$, $^3J_{PC}$ C$_{PhAl\_para}$ overlap with C$_{PhAl\_meta}$), 131,9 (d, $^3J_{PC} = 13.1$ Hz, C$_{PPh2\_meta}$), 129.1 (d, $^1J_{PC} = 98.8$ Hz, C$_{PPh2\_ipso}$), 128.8 (d, $^3J_{PC} = 10.9$ Hz, C$_{PhAl\_meta}$), 121.5 (d, $^1J_{PC} = 72.5$ Hz, C$_{CMe2}$), 21.1 (m, C$_{CMe2}$). ^{31}P{^{1}H} NMR (121 MHz, 298 K, C$_6$D$_6$, ppm): $\delta = 36.4$ (s). ^{19}F NMR (282 MHz, 298 K, C$_6$D$_6$, ppm): $\delta = -119.4$ (m, C$_6$F$_{5\_meta}$), -156.1 (t, $^2J_{FF} = 19.8$ Hz C$_6$F$_{5\_ortho}$), -162.0 (m, C$_6$F$_{5\_para}$). IR (ATR, cm^{-1}): see the Supporting Information. Elemental analysis: Due to the high fluorine content no satisfactory elemental analysis could be obtained.

General protocol for the synthesis of the compounds 3^R: In a Young capped NMR or Schlenk tube, **2^R** is dissolved in C$_6$D$_6$ or toluene and degassed. The solution is then gassed with CO$_2$ (4 bar) and heated to 60 °C for 4 days. Afterward, the solvent is evaporated to furnish the products. See the Supporting Information for details.

3^{Me} (16 mg, 72%) colorless crystalline solid. M.p. (decomp.): 143 °C. ^{1}H NMR (300 MHz, 298 K, THF-D8, ppm): $\delta = 7.94$–7.9 (m, H$_{PhAl\_ortho}$, 1H), 7.78–7.72 (m, H$_{Ar}$, 2H), 7.64–7.57 (m, H$_{Ph2\_meta}$, 4H), 7.56–7.48 (m, H$_{Ph2\_otho}$, 4H), 7.26–7.20 (m, H$_{Ar}$, 1H), 7.18–7.11 (m, H$_{Ar}$, 1H), 1.65 (d, $^3J_{PH} = 17.6$ Hz, H$_{CMe2}$, 6H), -1.14 (s, H$_{AlMe2}$, 6H). ^{13}C{^{1}H} NMR (75 MHz, 298 K, THF-D$_8$, ppm): $\delta = 168.30$ (s, C$_{CO2}$), 139.8 (d, $^2J_{PC} = 22.5$ Hz, C$_{PhAl\_ortho}$), 135.0 (d, $^4J_{PC} = 8.5$ Hz, C$_{PPh2\_para}$), 134.9 (d, $^4J_{PC} = 3.0$ Hz, C$_{PhAl\_para}$), 132.0 (d, $^3J_{PC} = 4.0$ Hz, C$_{PhAl\_meta}$), 130.6 (d, $^2J_{PC} = 12.3$ Hz, C$_{PPh2\_ortho}$), 129.1 (d, $^3J_{PC} = 12.0$ Hz, C$_{PhAl\_meta}$), 127.1 (d, $^3J_{PC} = 13.3$ Hz, C$_{PPh2\_meta}$), 125.1 (d, $^1J_{PC} = 87.8$ Hz, C$_{PPh2\_ipso}$), 122.9 (d, $^1J_{PC} = 79.2$ Hz, C$_{CMe2}$), 25.1 (bs, C$_{CMe2}$). ^{31}P{^{1}H} NMR (121 MHz, 298 K, THF-D$_8$, ppm): $\delta = 30.6$ (s). IR (ATR, cm^{-1}): $\tilde{v} = 1675$ (s), see also the Supporting Information. Elemental analysis (%): (calcd., found for C$_{24}$H$_{26}$AlPO$_2$·0.5 C$_6$H$_6$); C (73.12, 72,98), H (6.59, 6.33).

3^{Et} (14.8 mg, 67%) colorless crystalline solid. M.p. (decomp.): 145 °C. ^{1}H NMR (300 MHz, 298 K, C$_6$D$_6$, ppm): $\delta = 8.27$–8.22 (m, H$_{PhAl\_ortho}$, 1H), 7.36–7.22 (m, H$_{PhAl\_meta}$, 3H), 7.14–7.20 (m, H$_{PhAl\_para}$, 1H), 7.06–6.88 (m, H$_{Ph2\_meta}$, 6H), 6.87–6.79 (m, H$_{Ph2\_otho}$, 4H), 1.51–1.41 (m, H$_{AlCH2CH3}$ overlap with H$_{CMe2}$ 12H), 0.38–0.27 (m, H$_{AlCH2CH3}$, 4H). ^{13}C{^{1}H} NMR (75 MHz, 298 K, C$_6$D$_6$, ppm): $\delta = 168.3$ (s, C$_{CO2}$), 139.9 (d, $^2J_{PC} = 22.1$ Hz, C$_{PhAl\_ortho}$), 134.9 (d, $^2J_{PC} = 16.7$ Hz, C$_{PPh2\_ortho}$), 134.4 (d, $^4J_{PC} = 8.0$ Hz, C$_{PPh2\_para}$), 133.7 (d, $^3J_{PC} = 8.7$ Hz, C$_{PPh2\_meta}$), 133.6 (d, $^4J_{PC} = 2.8$ Hz, C$_{PhAl\_para}$), 130.1 (d, $^1J_{PC} = 104.3$ Hz, C$_{PPh2\_ipso}$), 131.3 (d, $^3J_{PC} = 4.2$ Hz, C$_{PhAl\_meta}$), 129.6 (d, $^3J_{PC} = 11.9$ Hz, C$_{PhAl\_meta}$), 122.2 (d, $^1J_{PC} = 88.1$ Hz, C$_{PhAl\_ipso}$), 122.2 (d, $^1J_{PC} = 78.8$ Hz, C$_{CMe2}$), 48.6 (d, $^2J_{PC} = 41.0$ Hz, C$_{AlCH2CH3}$), 25.9 (s, C$_{AlCH2CH3}$), 21.6 (d, $^2J_{PC} = 2.6$ Hz, C$_{CMe2}$), 10.8 (bs, C$_{AlCH2CH3}$). ^{31}P{^{1}H} NMR (121 MHz, 298 K, C$_6$D$_6$, ppm): $\delta = 30.7$ (s). IR (ATR, cm^{-1}): $\tilde{v} = 1683$ (vs), see also the Supporting Information.

3^{tBu} (228 mg, 67%) colorless solid. M.p. (decomp.): 201 °C. ^{1}H NMR (300 MHz, 298 K, C$_6$D$_6$, ppm): $\delta = 8.32$–8.24 (m, H$_{PhAl\_ortho}$, 1H), 7.25–7.80 (m, H$_{Ar}$, overlap with C$_6$D$_6$, 1H), 7.96–6.86 (m, H$_{Ph2\_meta}$, 4H), 6.80–6.70 (m, H$_{Ph2\_otho}$, 4H), 1.37 (d, $^3J_{PH} = 17.6$ Hz, H$_{CMe2}$, 6H), 1.27 (bs, H$_{CMe3}$, 18H). ^{13}C{^{1}H} NMR (75 MHz, 298 K, C$_6$D$_6$, ppm): $\delta = 169.1$ (s, C$_{CO2}$), 140.7 (d, $^2J_{PC} = 23.0$ Hz, C$_{PhAl\_ortho}$), 135.8 (d, $^2J_{PC} = 17.2$ Hz, C$_{PPh2\_ortho}$), 134.1 (d, $^4J_{PC} = 8.2$ Hz, C$_{PPh2\_para}$), 133.3 (d, $^4J_{PC} = 3.0$ Hz, C$_{PhAl\_para}$), 130.7 (d, $^3J_{PC} = 4.0$ Hz, C$_{PhAl\_meta}$), 129.4 (d, $^3J_{PC} = 11.4$ Hz, C$_{PPh2\_meta}$), 126.9 (d, $^3J_{PC} = 13.2$ Hz, C$_{PhAl\_meta}$), 126.0 (d, $^1J_{PC} = 87.0$ Hz, C$_{CMe2}$), 33.3 (s, C$_{CMe3}$), 24.6 (d, $^2J_{PC} = 3.8$ Hz, C$_{CMe2}$). ^{31}P{^{1}H} NMR (121 MHz, 298 K, C$_6$D$_6$, ppm): $\delta = 32.5$ (s). IR (ATR, cm^{-1}): $\tilde{v} = 1673$ (vs), see also the Supporting Information. Elemental analysis (%): (calcd., found for C$_{30}$H$_{38}$AlPO$_2$·C$_6$H$_6$); C (76.30, 76.16), H (7.82, 7,98).

3^{Mes} (12.2 mg, 57%) colorless crystalline solid. M.p. (decomp.): 150 °C. ^{1}H NMR (400 MHz, 298 K, C$_6$D$_6$, ppm): $\delta = 8.48$–8.44 (m, H$_{PhAl\_ortho}$, 1H), 7.07–6.99 (m, H$_{Ar}$, 6H), 6.94–6.88 (m, H$_{Ar}$, 3H), 6.88–6.85 (m, H$_{Mes\_meta}$, 4H) 6.85–6.73 (m, H$_{Ar}$, 1H), 6.77–6.71 (m, H$_{Ar}$, 5H), 2.52 (bs, H$_{Mes\_ortho}$, 12H), 2.27 (s, H$_{Mes\_para}$, 6H), 1.30 (d, $^3J_{PH} = 18.2$ Hz,

Chem. Eur. J. **2023**, e202303380 (8 of 10)

© 2023 The Authors. Chemistry - A European Journal published by Wiley-VCH GmbH

Chemistry–A European Journal

Research Article
doi.org/10.1002/chem.202303380

Chemistry Europe
European Chemical
Societies Publishing

H_{CMe2}, 6H). $^{13}C\{^1H\}$ NMR (75 MHz, 298 K, C_6D_6, ppm): $\delta = 168.5$ (s, C_{CO2}), 145.9 (s, C_{Mes_ipso}), 140.2 (d, $^2J_{PC} = 21.5$ Hz, C_{PhAl_ortho}), 135.4 (s, C_{Mes_para}), 133.3 (d, $^4J_{PC} = 8.3$ Hz, C_{PPh2_para}), 132.8 (d, $^4J_{PC} = 2.7$ Hz, C_{PhAl_para}), 132.1 (d, $^2J_{PC} = 9.5$ Hz, C_{PPh2_ortho}), 131.3 (d, $^3J_{PC} = 3.9$ Hz, C_{PhAl_meta}), 129.0 (d, $^3J_{PC} = 11.6$ Hz, C_{PPh2_meta}), 127.1 (s, C_{Mes_meta}) 125.9 (d, $^3J_{PC} = 13.4$ Hz, C_{PhAl_meta}), 125.0 (d, $^1J_{PC} = 86.1$ Hz, C_{CMes}), 124.4 (s, C_{Mes_ortho}), 48.1 (d, $^2J_{PC} = 45.0$ Hz, C_{PhAl_ortho}), 25.8 (s, C_{Me_ortho}), 21.7 (s, C_{Me_para}) 21.0 (d, $^2J_{PC} = 10.7$ Hz, C_{CMe2}). $^{31}P\{^1H\}$ NMR (121 MHz, 298 K, C_6D_6, ppm): $\delta = 33.3$ (s). IR (ATR, cm^{-1}): $\tilde{\upsilon} = 1682$ (m), see also the Supporting Information. Elemental analysis (%): (calcd., found for $C_{40}H_{42}AlPO_2$; C (78.41, 77.93), H (6.91, 6.62).

3^{C6F5} in the form of a light brown solid. M.p. (decomp.): 130 °C. $^{31}P\{^1H\}$ NMR (121 MHz, 298 K, THF-D_8, ppm): $\delta = 26.4$ (s). ^{19}F NMR (282 MHz, 298 K, THF-D_8, ppm): $\delta = -127.9$ (m, $C_6F_{5\_meta}$), -140.13 (m, $C_6F_{5\_ortho}$), -160.5 (m, $C_6F_{5\_para}$). Due to the poor solubility of **3^{C6F5}**, clean ^1H and ^{31}C NMR spectra could not be obtained. IR (ATR, cm^{-1}): $\tilde{\upsilon} = 1487$ (vs), see also the Supporting Information. Elemental analysis: Due to the high fluorine content no satisfactory elemental analysis could be obtained.

Catalytic reactions: For the catalytic reactions **2^R** or **4^R** and C_6Me_6 (as internal standard) were dissolved in benzene-d_6 (0.6 ml) in a Young capped NMR tube. Then HBPin (30–300 eq.) was added with an Eppendorf pipette. The mixtures were degassed and subsequently gassed with CO_2 (4 bar) by freezing four times the volume of one a Young capped NMR tube CO_2 into the reaction NMR tube. The mixtures were heated to 60 °C for 1–6 days. Conversions and reaction times are summarized in Table 4 and S2.

Crystallographic details: Deposition Numbers 2213402 (for $(C_6F_5)_2$GaCl·Tol), 2213044 (for **2^{Me}**), 2251423 (for **2^{Et}**), 2213046 (for **2^{Mes}**), 2213050 (for **2^{C6F5}**), 2213049 (for **3^{Me}**), 2213047 (for **3^{tBu}**) 2213045 (for **4^{Et}**), 2213048 (for **4^{tBu}**) and 2219891 (for **4^{C6F5}**) contain the supplementary crystallographic data for this paper. These data are provided free of charge by the joint Cambridge Crystallographic Data Centre and Fachinformationszentrum Karlsruhe Access Structures service.

Computational details: Geometry optimizations of the molecules were performed without symmetry constraints using the Gaussian16 (RevB.01) suite of programs[32] at the dispersion-corrected B3LYP[33]-D3[34]/def2-SVP[35] level including solvent effects (solvent = benzene) with the Polarization Continuum Model (PCM) method.[36] Reactants and adducts were characterized by frequency calculations and have positive definite Hessian matrices. Transition states show only one negative eigenvalue in their diagonalized force constant matrices, and their associated eigenvectors were confirmed to correspond to the motion along the reaction coordinate under consideration using the Intrinsic Reaction Coordinate (IRC) method.[37] The interaction between CO_2 and the title compounds in the transition states was analyzed with the Energy Decomposition Analysis method (see details in the Supporting Information).[38]

Supporting Information

For the preparation of $(C_6F_5)_2$GaCl, further experimental details, comprehensive listings of the IR data, NMR spectra and computational details, see Supporting Information. The authors have cited additional references within the Supporting Information.[39–43]

Conflict of Interests

The authors declare no conflict of interests.

Data Availability Statement

The data that support the findings of this study are available in the supplementary material of this article.

[1] National Oceanic and Atmospheric Administration, Global monitoring Laboratory https://keelingcurve.ucsd.edu/ (accessed 14. september 2023).

[2] a) M. D. Burkart, N. Hazari, C. L. Tway, E. L. Zeitler, *ACS Catal.* **2019**, *9*, 7937–7956; b) S. Dabral, T. Schaub, *Adv. Synth. Catal.* **2019**, *361*, 223–246; c) H.-Q. Liang, T. Beweries, R. Francke, M. Beller, *Angew. Chem. Int. Ed.* **2022**, *61*, e202200723.

[3] a) G. I. Nikonov, *ACS Catal.* **2017**, *7*, 7257–7266; b) W. Li, X. Ma, M. G. Walawalkar, Z. Yang, H. W. Roesky, *Coord. Chem. Rev.* **2017**, *350*, 14–29.

[4] C. Ni, X. Ma, Z. Yang, H. W. Roesky, *Eur. J. Inorg. Chem.* **2022**, *2022*, e202100929.

[5] a) D. Franz, C. Jandl, C. Stark, S. Inoue, *ChemCatChem* **2019**, *11*, 5275–5281; b) C.-C. Chia, Y.-C. Teo, N. Cham, S. Y.-F. Ho, Z.-H. Ng, H.-M. Toh, N. Mézailles, C.-W. So, *Inorg. Chem.* **2021**, *60*, 4569–4577.

[6] a) F.-G. Fontaine, D. W. Stephan, *Curr. Opin. Green Sustain. Chem.* **2017**, *3*, 28–32; b) Md. N. Khan, Y. van Ingen, T. Boruah, A. McLauchlan, T. Wirth, R. L. Melen, *Chem. Sci.* **2023**, Advance Article (DOI: 10.1039/d3sc03907b).

[7] a) M.-A. Courtemanche, M.-A. Légaré, L. Maron, F.-G. Fontaine, *J. Am. Chem. Soc.* **2013**, *135*, 9326–9329; b) A. Tlili, A. Voituriez, A. Marinetti, P. Thuéry, T. Cantat, *Chem. Commun.* **2016**, *52*, 7553–7555; c) R. Declercq, G. Bouhadir, D. Bourissou, M.-A. Légaré, M.-A. Courtemanche, K. S. Nahi, N. Bouchard, F.-G. Fontaine, L. Maron, *ACS Catal.* **2015**, *5*, 2513–2520; d) A. Ramos, A. Antiñolo, F. Carrillo-Hermosilla, R. Fernández-Galán, *Inorg. Chem.* **2020**, *59*, 9998–10012.

[8] A. Ramos, A. Antiñolo, F. Carrillo-Hermosilla, R. Fernández-Galán, A. Rodríguez-Diéguez, D. García-Vivó, *Chem. Commun.* **2018**, *54*, 4700–4703.

[9] a) M.-A. Courtemanche, J. Larouche, M.-A. Légaré, W. Bi, L. Maron, F.-G. Fontaine, *Organometallics* **2013**, *32*, 6804–6811; b) L. Werner, J. Hagn, J. Walpuski, U. Radius, *Angew. Chem. Int. Ed.* **2023**, e202312111.

[10] N. von Wolff, G. Lefèvre, J. C. Berthet, P. Thuéry, T. Cantat, *ACS Catal.* **2016**, *6*, 4526–4535.

[11] X. Chen, Y. Yang, H. Wang, Z. Mo, *J. Am. Chem. Soc.* **2023**, *145*, 7011–7020.

Chem. Eur. J. **2023**, e202303380 (9 of 10)

© 2023 The Authors. Chemistry - A European Journal published by Wiley-VCH GmbH

[12] a) D. W. Stephan, G. Erker, *Angew. Chem. Int. Ed.* **2010**, *49*, 46–76; b) D. W. Stephan, *J. Am. Chem. Soc.* **2015**, *137*, 10018–10032; c) D. W. Stephan, *Acc. Chem. Res.* **2015**, *48*, 306–316; d) D. W. Stephan, G. Erker, *Angew. Chem. Int. Ed.* **2015**, *54*, 6400–6441; e) D. W. Stephan, *Science* **2016**, *354*, aaf7229; f) G. C. Welch, R. R. S. Juan, J. D. Masuda, D. W. Stephan, *Science* **2006**, *314*, 1124–1126.

[13] a) J. Boudreau, M.-A. Courtemanche, F.-G. Fontaine, *Chem. Commun.* **2011**, *47*, 11131–11133; b) S. Roters, C. Appelt, H. Westenberg, A. Hepp, J. C. Slootweg, K. Lammertsma, W. Uhl, *Dalton Trans.* **2012**, *41*, 9033–9045; c) S. Roters, A. Hepp, J. C. Slootweg, K. Lammertsma, W. Uhl, *Chem. Commun.* **2012**, *48*, 9616–9618; d) F. Hengesbach, X. Jin, A. Hepp, B. Wibbeling, E.-U. Würthwein, W. Uhl, *Chem. Eur. J.* **2013**, *19*, 13901–13909; e) H. Klöcker, M. Layh, A. Hepp, W. Uhl, *Dalton Trans.* **2016**, *45*, 2031–2043; f) S. Styra, M. Radius, E. Moos, A. Bihlmeier, F. Breher, *Chem. Eur. J.* **2016**, *22*, 9508–9512; g) W. Uhl, J. S. Bruchhage, A. Hepp, J. Kösters, *Eur. J. Inorg. Chem.* **2016**, *2016*, 2721–2730; h) W. Uhl, M. Willeke, F. Hengesbach, A. Hepp, M. Layh, *Organometallics* **2016**, *35*, 3701–3712; i) K. Martinewski, T. Holtrichter-Rößmann, C. Rösener, A. Hepp, E.-U. Würthwein, W. Uhl, *Chem. Eur. J.* **2017**, *23*, 6129–6141; j) W. Uhl, M. Willeke, A. Hepp, D. Pleschka, M. Layh, *Z. Anorg. Allg. Chem.* **2017**, *643*, 387–397; k) M. Simon, M. Radius, H. E. Wagner, F. Breher, *Eur. J. Inorg. Chem.* **2020**, *2020*, 1906–1914; l) D. W. N. Wilson, J. Feld, J. M. Goicoechea, *Angew. Chem. Int. Ed.* **2020**, *59*, 20914–20918; m) T. W. Yokley, H. Tupkar, N. D. Schley, N. J. DeYonker, T. P. Brewster, *Eur. J. Inorg. Chem.* **2020**, *2020*, 2958–2967.

[14] a) A. Sarbajna, V. S. V. S. N. Swamy, V. H. Gessner, *Chem. Sci.* **2021**, *12*, 2016–2024; b) F. Krämer, M. Radius, A. Hinz, M. E. A. Dilanas, F. Breher, *Chem. Eur. J.* **2022**, *28*, e202103974; c) M. Radius, F. Breher, *Chem. Eur. J.* **2018**, *24*, 15744–15749; d) M. Radius, E. Sattler, H. Berberich, F. Breher, *Chem. Eur. J.* **2019**, *25*, 12206–12213.

[15] F. Krämer, J. Paradies, I. Fernández, F. Breher, *Nat. Chem.* **2023**, https://doi.org/10.1038/s41557-023-01340-9.

[16] a) B. Schaub, T. Jenny, M. Schlosser, *Tetrahedron Lett.* **1984**, *25*, 4097–4100; b) B. Schaub, M. Schlosser, *Tetrahedron Lett.* **1985**, *26*, 1623–1626; c) K. Korth, J. Sundermeyer, *Tetrahedron Lett.* **2000**, *41*, 5461–5464.

[17] N. Wiberg, *Lehrbuch der Anorganischen Chemie*, 102nd Edition, De Gruyter, **2007**.

[18] C. Appelt, H. Westenberg, F. Bertini, A. W. Ehlers, J. C. Slootweg, K. Lammertsma, W. Uhl, *Angew. Chem. Int. Ed.* **2011**, *123*, 4011–4014.

[19] a) D. Yepes, P. Jaque, I. Fernández, *Chem. Eur. J.* **2016**, *22*, 18801–18809; b) J. J. Cabrera-Trujillo, I. Fernández, *Chem. Eur. J.* **2018**, *24*, 17823–17831; c) J. J. Cabrera-Trujillo, I. Fernández, *Inorg. Chem.* **2019**, *58*, 7828–7836; d) J. J. Cabrera-Trujillo, I. Fernández, *J. Phys. Chem. A* **2019**, *123*, 10095–10101; e) I. Fernández, *Chem. Commun.* **2022**, *58*, 4931–4940.

[20] a) F. Ebner, L. M. Sigmund, L. Greb, *Angew. Chem. Int. Ed.* **2020**, *59*, 17118–17124; b) C. L. Shaves, N. Villegas-Escobar, E. R. Clark, I. M. Riddlestone, *Chem. Eur. J.* **2023**, *29*, e202203806.

[21] a) M. D. Anker, M. Arrowsmith, P. Bellham, M. S. Hill, G. Kociok-Köhn, D. J. Liptrot, M. F. Mahon, C. Weetman, *Chem. Sci.* **2014**, *5*, 2826–2830; b) C.-C. Chia, Y.-C. Teo, N. Cham, S. Y.-F. Ho, Z.-H. Ng, H.-M. Toh, N. Mézailles, C.-W. So, *Inorg. Chem.* **2021**, *60*, 4569–4577.

[22] a) J. A. B. Abdalla, I. M. Riddlestone, R. Tirfoin, S. Aldridge, *Angew. Chem. Int. Ed.* **2015**, *54*, 5098–5102; b) L. Liu, S.-K. Lo, C. Smith, J. M. Goicoechea, *Chem. Eur. J.* **2021**, *27*, 17379–17385.

[23] A. K. Swarnakar, S. M. McDonald, K. C. Deutsch, P. Choi, M. J. Ferguson, R. McDonald, E. Rivard, *Inorg. Chem.* **2014**, *53*, 8662–8671.

[24] W. Uhl, J. Wagner, D. Fenske, G. Baum, *Z. Anorg. Allg. Chem.* **1992**, *612*, 25–34.

[25] Y. Nie, P. Wang, H. Du, W. Meng, J. Yang, *Polym. Chem.* **2018**, *9*, 5014–5023.

[26] W. Uhl, M. Layh, I. Rhotert, A. Wollschläger, A. Hepp, *Z. Naturforsch. B* **2013**, *68*, 503–517.

[27] J. Backs, M. Lange, J. Possart, A. Wollschläger, C. Mück-Lichtenfeld, W. Uhl, *Angew. Chem. Int. Ed.* **2017**, *56*, 3094–3097.

[28] J. Koziskova, F. Hahn, J. Richter, J. Kožíšek, *Acta Chimi. Slov.* **2016**, *9*, 136–140.

[29] O. V. Dolomanov, L. J. Bourhis, R. J. Gildea, J. A. K. Howard, H. Puschmann, *J. Appl. Crystallogr.* **2009**, *42*, 339–341.

[30] G. Sheldrick, *Acta Crystallogr. Section A* **2015**, *71*, 3–8.

[31] G. Sheldrick, *Acta Crystallogr. Section C* **2015**, *71*, 3–8.

[32] Gaussian 16, Revision B.01, M. J. Frisch, G. W. Trucks, H. B. Schlegel, G. E. Scuseria, M. A. Robb, J. R. Cheeseman, G. Scalmani, V. Barone, G. A. Petersson, H. Nakatsuji, X. Li, M. Caricato, A. V. Marenich, J. Bloino, B. G. Janesko, R. Gomperts, B. Mennucci, H. P. Hratchian, J. V. Ortiz, A. F. Izmaylov, J. L. Sonnenberg, D. Williams-Young, F. Ding, F. Lipparini, F. Egidi, J. Goings, B. Peng, A. Petrone, T. Henderson, D. Ranasinghe, V. G. Zakrzewski, J. Gao, N. Rega, G. Zheng, W. Liang, M. Hada, M. Ehara, K. Toyota, R. Fukuda, J. Hasegawa, M. Ishida, T. Nakajima, Y. Honda, O. Kitao, H. Nakai, T. Vreven, K. Throssell, J. A. Montgomery, Jr., J. E. Peralta, F. Ogliaro, M. J. Bearpark, J. J. Heyd, E. N. Brothers, K. N. Kudin, V. N. Staroverov, T. A. Keith, R. Kobayashi, J. Normand, K. Raghavachari, A. P. Rendell, J. C. Burant, S. S. Iyengar, J. Tomasi, M. Cossi, J. M. Millam, M. Klene, C. Adamo, R. Cammi, J. W. Ochterski, R. L. Martin, K. Morokuma, O. Farkas, J. B. Foresman, and D. J. Fox, Gaussian, Inc., Wallingford CT, **2016**.

[33] a) A. D. Becke, *J. Chem. Phys.* **1993**, *98*, 5648; b) C. Lee, W. Yang, R. G. Parr, *Phys. Rev. B* **1998**, *37*, 785; c) S. H. Vosko, L. Wilk, M. Nusair, *Can. J. Phys.* **1980**, *58*, 1200.

[34] S. Grimme, J. Antony, S. Ehrlich, H. Krieg, *J. Chem. Phys.* **2010**, *132*, 154104.

[35] F. Weigend, R. Ahlrichs, *Phys. Chem. Chem. Phys.* **2005**, *7*, 3297.

[36] a) S. Miertuš, E. Scrocco, J. Tomasi, *Chem. Phys.* **1981**, *55*, 117; b) J. L. Pascual-Ahuir, E. Silla, I. Tuñón, *J. Comput. Chem.* **1994**, *15*, 1127; c) V. Barone, M. Cossi, *J. Phys. Chem. A* **1998**, *102*, 1995.

[37] C. Gonzalez, H. B. Schlegel, *J. Phys. Chem.* **1990**, *94*, 5523.

[38] a) F. M. Bickelhaupt, E. J. Baerends, in *Reviews in Computational Chemistry*, (Eds. K. B. Lipkowitz, D. B. Boyd), Wiley-VCH: New York, **2000**, Vol. 15, pp. 1–86; b) M. von Hopffgarten, G. Frenking, *WIREs Comput. Mol. Sci.* **2012**, *2*, 43–62; c) I. Fernández, in *Applied Theoretical Organic Chemistry*, (Ed. D. J. Tantillo), World Scientific, New Jersey, **2018**, pp. 191.

[39] M. P. Mitoraj, A. Michalak, T. Ziegler, *J. Chem. Theory Comput.* **2009**, *5*, 962.

[40] a) G. te Velde, F. M. Bickelhaupt, E. J. Baerends, C. Fonseca Guerra, S. J. A. van Gisbergen, J. G. Snijders, T. Ziegler, *J. Comput. Chem.* **2001**, *22*, 931–967; b) *ADF2020*, SCM, Theoretical Chemistry, Vrije Universiteit, Amsterdam, The Netherlands, http://www.scm.com.

[41] J. G. Snijders, P. Vernooijs, E. J. Baerends, *At. Data Nucl. Data Tables* **1981**, *26*, 483.

[42] J. Krijn, E. J. Baerends, *Fit Functions in the HFS-Method*, Internal Report (in Dutch), Vrije Universiteit Amsterdam, The Netherlands, **1984**.

[43] a) E. van Lenthe, E. J. Baerends, J. G. Snijders, *J. Chem. Phys.* **1993**, *99*, 4597; b) E. van Lenthe, E. J. Baerends, J. G. Snijders, *J. Chem. Phys.* **1994**, *101*, 9783; c) E. van Lenthe, A. Ehlers, E. J. Baerends, *J. Chem. Phys.* **1999**, *110*, 8943.

RESEARCH ARTICLE

E = Al, Ga
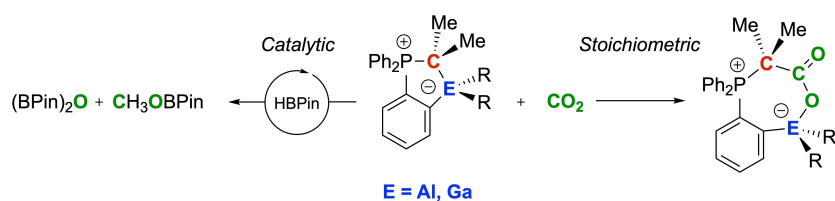
Stoichiometric vs. Catalytic: The herein reported aluminum and gallium/carbon-based ambiphiles, a new class of hidden frustrated Lewis pairs consisting of a phosphorus ylide featuring an aluminum or gallium fragment in the *ortho* position of a phenyl ring scaffold, react stoichiometrically with CO_2 forming the stable adducts but also act as an efficient catalyst for the reduction of CO_2 mediated by HBpin.

Dr. F. Krämer, Prof. Dr. J. Paradies, Prof. Dr. I. Fernández*, Prof. Dr. F. Breher*

1 – 11

Quo Vadis CO₂ Activation: Catalytic Reduction of CO₂ to Methanol Using Aluminum and Gallium/Carbon-based Ambiphiles